ChemPubSoc Europe

DOI: 10.1002/chem.201503437

CHEMISTRY A European Journal Full Paper

Metal–Organic Frameworks

Reversed Crystal Growth of RHO Zeolitic Imidazolate Framework (ZIF)

Katherine Self, Michael Telfer, Heather F. Greer, and Wuzong Zhou*[a]

Abstract: RHO zeolitic imidazolate framework (ZIF), $Zn_{1.33}(O.OH)_{0.33}(nim)_{1.167}(pur)$, crystals with a rhombic dodecahedral morphology were synthesized by a solvothermal process. The growth of the crystals was studied over time using scanning electron microscopy (SEM), transmission electron microscopy (TEM), powder X-ray diffraction (PXRD) and Brunauer–Emmett–Teller (BET) analyses, and a reversed crystal growth mechanism was revealed. Initially, precursor materials joined together to form disordered aggregates, which then underwent surface recrystallization forming a core–shell structure, in which a disordered core is encased in a layer of denser, less porous crystal. When the growth continued, the shell became less and less porous, until it was a layer of true single crystal. The crystallization then extended from the surface to the core over a six-week period until, eventually, true single crystals were formed.

Introduction

Metal–organic frameworks (MOFs) are highly porous solids generally obtained through solvothermal synthesis.[1] They consist of metal-containing inorganic clusters joined by organic linkers and have been of high interest recently due to their large range of potential applications in areas, such as catalysis,[2] sensing[3] and drug delivery.[4]

Zeolitic imidazolate frameworks (ZIFs) are a sub-class of MOFs, which have exceptionally high thermal and chemical stabilities and high surface areas and so are extremely promising for absorption applications.[5] ZIFs are composed of metal cations tetrahedrally coordinated by imidazolate linkers and have distinct topologies dependent on the linkers used. Herein, a relatively new ZIF developed at our university in 2012,[6] which has both purinate (pur) and 2-nitroimidazolate (nim) acting as the linkers between zinc cation centres and has the chemical formula, $Zn_{1.33}(O.OH)_{0.33}(nim)_{1.167}(pur)$, was synthesized. Mixed linker ZIFs (i.e., those with more than one ligand) are able to form structures, which would not be possible with a single linker, and in which the kinetic stability of the final structure is a direct result of the linker combinations.[7] The pur ligand is usually responsible for forming the LTA topology,[8] but the inclusion of the second, nim, ligand interrupts the link-to-link interactions and instead causes the formation of the GME or RHO topologies depending on the zinc source.[6] In the present case, zinc nitrate was used as the metal source, hence, this ZIF adopts a RHO-type topology, similar to that of the well-studied, single linker, ZIF-11 ($Zn(bzim)_2$), and so will be referred to during this work as RHO ZIF. In this structure, each super-cage is connected to six others through eight-membered rings (Figure 1). The central super-cage is not connected to any of its nearest-neighbour super-cages, which are located by its diagonal six-membered rings, but instead to six others further by the eight-membered rings (shown in Figure 1 a). This means that there are two interpenetrating (but not connected) arrays of super-cages throughout the structure.

Many MOF and ZIF crystals appear to be single crystals due to their perfect outer appearance and highly symmetric polyhedral morphology. Therefore, their growth has often been assumed to follow the classical, "bottom-up", route and has been unstudied. This classical crystal growth theory, which was established over a century ago and is described by the Bravais–Friedel–Donnay–Harker (BFDH) law,[11] Ostwald ripening[12] and Hartman–Perdok theory,[13] describes the growth of free

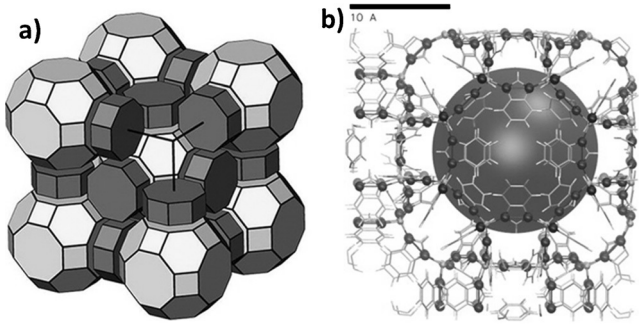

Figure 1. a) The RHO-type topology.[9] b) Structural model of ZIF-11 viewed through one of the connecting eight-membered rings.[10]

[a] K. Self, M. Telfer, Dr. H. F. Greer, Prof. W. Z. Zhou
EaStCHEM, School of Chemistry, University of St Andrews
St Andrews KY16 9ST (UK)
Fax: (+44) 1334-468308
E-mail: wzhou@st-andrews.ac.uk

Supporting information for this article is available on the WWW under http://dx.doi.org/10.1002/chem.201503437.

crystals from a single nucleus through layer-by-layer deposition of the building units. This has been proven to not always be the true growth route, however, as in the case of MOF-5, which has been shown to follow reversed crystal growth instead,[14] in which growth occurs by aggregation of nanocrystallites followed by surface re-crystallisation. The crystallisation then extends from the surface to the core until true single crystals are formed. This non-classical crystal growth mechanism, first reported in 2007 for the zeolite analcime,[15] has been found to be the true growth process of many materials, which had previously been believed to follow the classical route. Examples include metals and metal oxides,[16] perovskites,[17] organic crystals[18] and other zeolites.[19] Through these studies, it has become clear that the aggregation of precursor molecules/ions at an early stage is the key step for reversed crystal growth. Synthetic solutions for MOFs always contain a combination of inorganic and organic precursors, which generally have strong interactions between them. This would enhance fast aggregation before individual free crystals are developed, therefore, leading to reversed crystal growth.

The wealth of potential applications of such a material makes it essential to be aware of the mechanism by which RHO ZIF crystals grow, because only by truly understanding their growth can we tailor their morphology to maximise the desirable properties. Herein, the growth of highly symmetric crystals of the Zn-based RHO ZIF is studied over time, uncovering a new example of a material, which follows a non-classical crystal growth mechanism and giving a deeper understanding of the ZIF's properties.

Results and Discussion

The growth of RHO ZIF crystals was initially studied over time using SEM analysis. It was found that at the earliest growth time of 1 h, particles with an average diameter of approximately 500 nm appeared, forming some loose clusters (Figure 2a), which start to aggregate into larger particles, some even displaying a pseudo-rhombic dodecahedral shape by three hours (Figure 2b). This is not the first time we have observed the existence of polycrystalline particles with a highly symmetric polyhedral morphology, which cannot be explained by the classical theories of polyhedral formation during crystal growth. This phenomenon can probably be attributed to an interaction between the nanocrystallites. However, more experiments and theoretical studies must be done before the mechanism can be fully understood.

XRD pattern of the three-hour sample revealed that these aggregates already display a crystalline phase with a low crystallinity that can be indexed to the cubic phase $Zn_{1.33}(O.OH)_{0.33}(nim)_{1.167}(pur)$ (i.e., RHO ZIF) with the unit-cell parameter $a = 29.044$ Å and space group *Im*-3*m* (Figure 3a).

It is known that crystal nucleation in ZIFs can be caused by the addition of a non-solvent, creating an environment, in which the reactants are unstable.[7] In this case, methanol was added into the solution, reducing the stability of the reactants[20] and causing the precipitation of products at relatively short reaction times, explaining why RHO ZIF particles can be produced in as little as three hours.

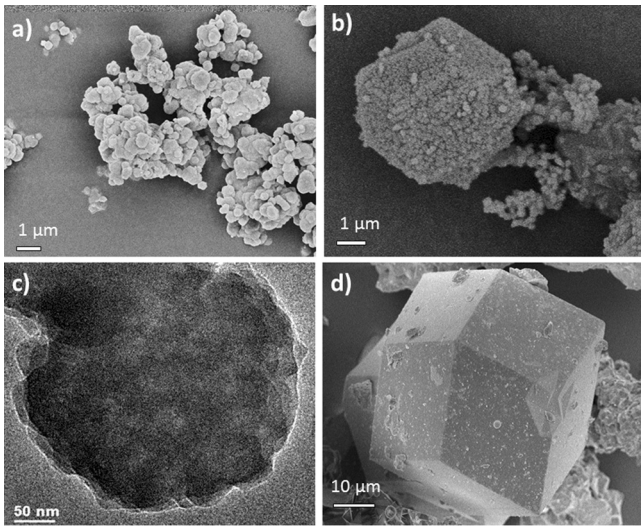

Figure 2. TEM and SEM images of the specimens during the growth of RHO ZIF crystals with different incubation times of a) one hour, b, c) three hours and d) three weeks.

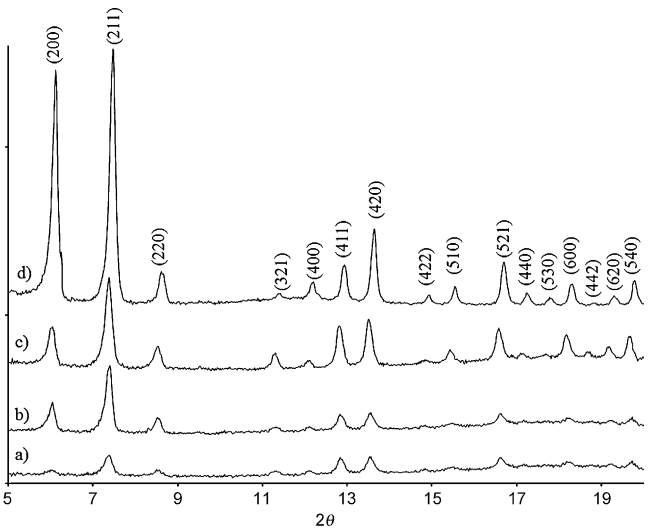

Figure 3. PXRD patterns of RHO ZIF samples grown over a) three hours, b) 24 hours, c) three weeks and d) six weeks. The reflections in d) are indexed to the cubic $Zn_{1.33}(O.OH)_{0.33}(nim)_{1.167}(pur)$ phase.

It was revealed that the individual spherical particles, approximately 500 nm in size, as shown in Figure 2a, are not single crystals. The TEM image displayed in Figure 2c shows a typical spherical particle from the three-hour sample, showing the nature of aggregation of smaller particles approximately 50 nm in diameter. It can be seen that the density of the aggregate is not uniform by the varying contrast in the image (the darker the region, the greater the mass thickness). Unfortunately, due to the presence of organic components within the RHO ZIF structure (causing it to break down under the high-intensity electron beam), it was extremely difficult to attain any high-resolution (HR) TEM images or selected-area

electron-diffraction (SAED) patterns to confirm the crystallinity of these nanoparticles and whether or not they were disordered. However, by using the Scherrer equation,[21] the average size of crystallites in the three-hour sample was determined from the corresponding XRD pattern to be approximately 35–40 nm, calculated from the (211), (411) and (420) peaks, which appear to match with the TEM images taken. This result indicates that the first step of the formation of RHO ZIF was disordered aggregation of the precursor molecules. Multiple nucleation and early-stage crystal growth then took place inside these amorphous soft-matter aggregates instead of developing free crystals in the synthetic solution.

Finally, after an incubation period of three weeks (Figure 2d) the crystals appeared to have a perfect polyhedral appearance, resembling that of a single crystal, displaying their final, rhombic dodecahedral morphology with a size range from 15 to 50 μm. This morphology, with 12 exposed {110} facets, is typical for ZIFs with the RHO topology. However, the intensity of the (110) peak for the RHO ZIF is too low to be observed, which is not the case for other ZIFs with the same topology. This is due to the presence of the two different linkers in the RHO ZIF structure. In the RHO framework-type, there are two individual linker sites, which exist in a 1:1 ratio connecting the supercages. In single-linker ZIFs, such as ZIF-11, both sites are occupied by the same linker, whereas in the RHO ZIF the nim ligands occupy one site and the pur ligands occupy the other, increasing the symmetry of the framework topology from P-type to I-type with an approximately doubled unit-cell dimension,[6] which decreases the intensity of the (110) peak and causes the intensity of the (220) to increase instead.

The intensity of the peaks in the XRD patterns increased with growth time, indicating an increase in the crystallinity of the RHO ZIF particles (Figure 3). A shoulder can be observed in the (200) peak at the longest growth time (Figure 3d), which is likely to be a result of two peaks overlapping due to the intergrowth, or interpenetration, of frameworks within the ZIF structure, evidence of which was observed in the current work across a range of growth times (Figure S1 in the Supporting Information). This interpenetration is allowed for many high-symmetry topologies and is frequently observed when long linkers (such as those used in the current work) are employed.[22]

However, when the particles with the seemingly single crystal outer appearance were crushed and studied again, more closely, it could be seen that they were not single crystals, but actually consisted of a "core–shell" structure, in which a disordered core is encased in a thin layer of single crystal (Figure 4). At a growth time of 24 h, the particles already appear single-crystal-like (Figure 4a). But when these particles were crushed, the porous, disordered core can be seen clearly by SEM analysis (Figure 4b). Moreover, when the outer surface of the particles was more closely examined, it became clear that even the outer layer is not quite single crystal, but is actually still porous (although it appears much denser than the core). This was also observed in cubic, "pomegranate-like" MOF-5 particles, in which the core and shell were shown to have different tiers of porosity.[23] Therefore, the particles are mainly polycrystalline. The average size of crystallites within the 24 h particles has been determined to be around 47 nm from the corresponding XRD peaks, calculated from the (200), (211) and (420) reflections.

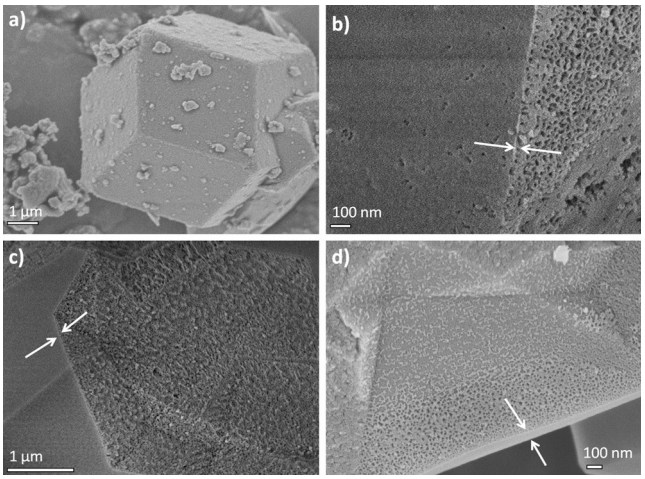

Figure 4. a) SEM image of typical RHO ZIF particle at 24 h. SEM images also shown of crushed particles grown over b) 24 hours, c) 4 days and d) 7 days. The arrows in b, c) and d) indicate the thickness of the outer shell.

The porosity of the 24-hour sample was determined by N_2 adsorption at 77 K (Figure S2 in the Supporting Information). The N_2 adsorption/desorption isotherm displays a type H_4 hysteresis loop indicating a mesoporous material with narrow, slit-like pores. The material was determined to have a Brunauer–Emmett–Teller (BET) surface area of 241 $m^2 g^{-1}$ with a maximum N_2 uptake of 5.95 $mmol\,g^{-1}$ and pore volume of 0.094 $cm^3 g^{-1}$. These values are smaller than those previously reported for $Zn_{1.33}(O,OH)_{0.33}(nim)_{1.167}(pur)$ with the RHO topology, which is likely to be due to the incomplete crystallization process. Kahr et al. reported a maximum N_2 uptake of 6.5 $mmol\,g^{-1}$, which is higher than the 24 h sample in the present work, but is still lower than the 10 $mmol\,g^{-1}$ value, predicted to be possible by their grand canonical Monte Carlo (GCMC) simulation.[6] Therefore, it may be the case that the RHO ZIF crystals they analysed, which were grown over seven days, were also not fully single crystalline.

When a crystal grown over four days was crushed open, the distinction between surface and core became more evident (Figure 4c). The very thin surface layer, indicated by the white arrows, has increased in crystallinity to the point that it now appears single crystalline, whereas the core is still highly disordered. When the growth time was increased further to seven days (Figure 4d), the core–shell structure was still apparent, but the thickness of the crystalline outer shell had increased when the crystallization was extending from the surface to the core. This was further confirmed by the (200) peak intensity in the PXRD patterns (Figure 3), which increases significantly over time relative to the other peaks, implying growth along the $<200>$ zone axes. Because the outer morphology and size of the crystals did not change significantly over time, this growth (increase in crystallinity) must be occurring primarily along the inner surface of the single-crystal shell, in which the vertices are the sites, which present the lowest energy. Therefore, the

thickness of the shell increases the fastest along the <100> directions, but because the (100) peak is a systematic absence for this structure, the intensity of the (200) peak greatly increases over time.

Further evidence of the disordered core was observed by TEM analysis. Figure 5 displays a TEM image of a fragment of a particle in the 48-hour sample. The top right edge, indicated by the arrow, is flat and has a darker contrast, implying that

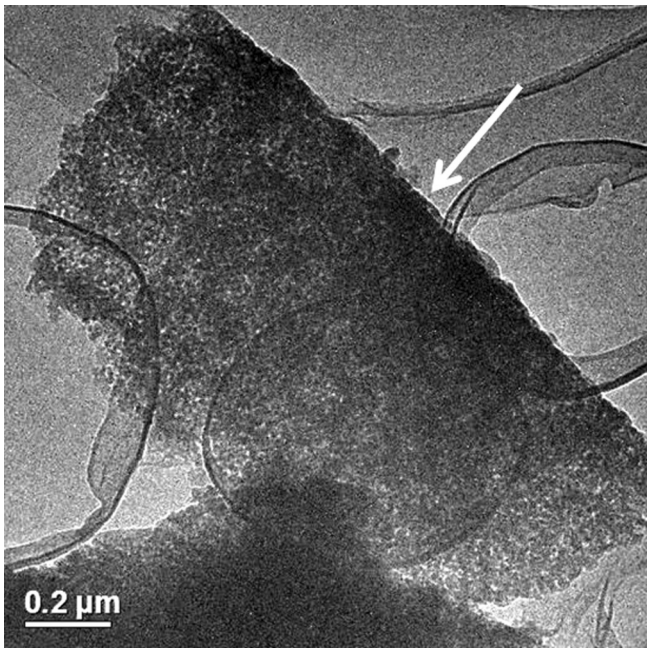

Figure 5. TEM image of a surface fragment of particle in the 48-hours sample displaying the disordered core underneath the dark contrast shell at the top right edge (indicated by the arrow).

this edge is probably the shell of the particle. It is evident from the variations in contrast within the lower part of the fragment that it is porous, polycrystalline with a low density. It was noticed that there is no clear line between the shell and the inner particles. Unfortunately, the crystal structure of RHO ZIF was very sensitive to the electron beam and decomposed immediately when the particles were exposed to it. Therefore, it was not possible to obtain SAED patterns or HRTEM images of this structure.

These results provide clear evidence that the growth of RHO ZIF crystals does not follow the classical mechanism, in which growth occurs by layer-by-layer deposition on a single nucleus. If that were the case, the crystals would have a single-crystal cross-section at all stages in the growth process. But in the present work, the growth of RHO ZIF appears to follow the reversed crystal growth mechanism, in which the first stage is the formation of disordered aggregates, which then undergo surface recrystallization followed by an extension of the crystallization towards the core, until a true single crystal is eventually formed. The reason this formation of aggregates is favoured is believed to be due to the strong interactions between the precursor molecules/ions. At a very early stage in the development of crystals, two processes are in competition: a process of nucleation followed by growth of free crystals in a solution and a process of aggregation of precursor molecules/ions. When the interaction between precursor molecules/ions is strong, aggregation dominates, and the growth of free crystals in solution is suppressed. In the present work, although no long-chain directing agent was added, the interaction between Zn^{2+} cations with the organic precursors (2-nitroimidazole and purine) is so strong that they join together quickly to form disordered spherical particles before forming crystals.[24] However, the ratio of the components may not be the same as that of RHO ZIF, so these nanospheres undergo further assembly into large aggregates. It is unlikely that nucleation of RHO ZIF takes place in the solution, because the concentrations of the precursors in the solution are significantly reduced. Therefore, the nucleation of the ZIF can only occur within the disordered aggregates. The formation of a single-crystal shell arises, because the surface of the aggregates with less restricted space and easier mass transportation offers a large number of active sites for crystallisation.

The extension of crystallisation from the surface to the core proceeds by an Ostwald ripening process and is very slow. Two reasons for this are that the movement of organic molecules within the soft matter cores of the particles is difficult, and also that the construction of the ZIF structure is based on highly selective connections of Zn^{2+} ions with the organic linkers.

The final stage of reversed crystal growth is the formation of true single crystals and to determine conclusively that this is the true mechanism for the RHO ZIF crystals, it is important to find evidence of complete single crystals as the final growth stage. Therefore, the synthesis was repeated with an even longer incubation period of six weeks, whereupon the XRD pattern showed crystalline peaks with much higher intensities (Figure 3d). SEM images revealed more regular rhombic dodecahedral particles (Figure 6a). The particle size did not increase significantly during such a long growth time. When the crystals were crushed and analysed by SEM technique, there were no longer any particles with a core–shell structure observed (Figure 6b). Instead, the SEM images showed a single-crystal cross-section (white arrows in Figure 6b).

The porosity of the six-week sample was determined by N_2 adsorption at 77 K. The sorption isotherm displays a type H_4 hysteresis similar to that of the 24-hour sample (Figure S3 in

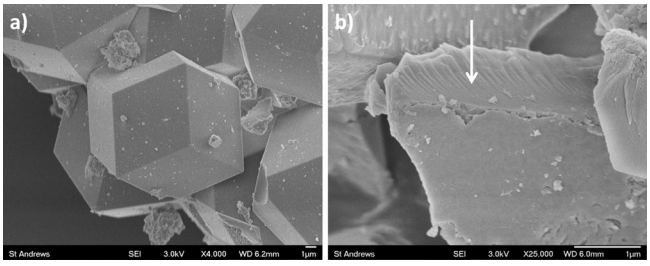

Figure 6. SEM images of RHO ZIF crystals in the six- week sample a) showing more regular rhombic dodecahedra and b) displaying crushed RHO ZIF particles. The white arrow indicates the single-crystal cross-section.

the Supporting Information), although the BET surface area had almost doubled to 417 $m^2 g^{-1}$, with a pore volume of 0.129 $cm^3 g^{-1}$ and an improved maximum N_2 uptake of 8.45 mmol g^{-1}. This uptake value is now higher than the previously reported literature value and much closer to the 10 mmol g^{-1} value, which was predicted to be possible by the GCMC simulation run by Kahr et al.[6] This is due to the fact that over the increased growth time, as the particles move towards becoming single crystals, they get closer to the simulated structure and become more ordered, increasing the pore volume and N_2 uptake (Figure 1a). It is also likely that when the core was more disordered (at the earlier growth stages), there were fewer clear channels through the crystals, prohibiting N_2 diffusion through the structure.

Summary of growth mechanism

Using the evidence gathered thus far, it is now possible to propose a new growth mechanism of the RHO ZIF crystals. Initially, in step 1, precursor molecules/ions form disordered spherical aggregates (Figure 7a), which then join together, in step 2, to give rise to porous particles with a pseudo-rhombic dodecahedral shape, made up of many embedded nanocrystallites of RHO ZIF (Figure 7b). In step 3 (Figure 7c), the surface of the disordered particles recrystallizes into a single-crystal shell with a perfect rhombic dodecahedral morphology, while the core remains disordered. In step 4, the recrystallization extends from the surface towards the core (Figure 7d), and finally, a real single-crystal state is achieved.

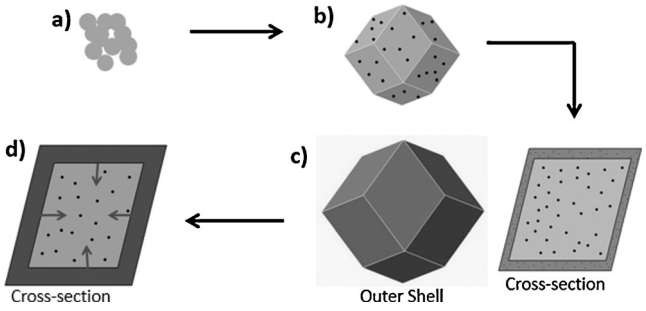

Figure 7. Schematic of proposed growth mechanism for rhombic dodecahedral RHO ZIF crystals. a) Disordered precursor materials form spherical aggregates. b) Aggregates join together to form porous pseudo-rhombic dodecahedral particles. c) Surface recrystallization occurs giving rise to a single-crystal outer shell encasing a porous core. d) Finally, the crystallization extends from the surface to the core until true single crystals are formed.

Conclusion

The results of this work clearly demonstrate that the classical bottom-up route of crystal growth, which was established over 100 years ago, is not always the appropriate explanation for the growth of highly symmetric polyhedral crystals. Herein, RHO ZIF has been shown to form rhombic dodecahedral crystals by following a reversed crystal-growth mechanism, in which the key step is aggregation of precursor molecules/ions at an early stage followed by surface recrystallization to form a single-crystal shell. It was reported by Curie and Wulff a long time ago that the equilibrium shape of a free crystal is that which minimizes its surface free energy.[25] According to this theory, the formation of the rhombic dodecahedral shell can be explained (even though the cores of the particles are still disordered), because a polyhedral morphology minimizes the surface free energy. However, the rhombic dodecahedral morphology of the particles appears before the formation of the single-crystal shell. This is not the first example of perfect polyhedral shape of polycrystalline particles and the reason has not yet been fully understood.

Discovering the true reversed crystal-growth mechanism of RHO ZIF gives us the opportunity to tune the microstructure and produce different morphologies at different growth times. For example, it is possible to fabricate polycrystalline particles with nanocrystallites embedded in an organic matrix, particles with a hierarchical pore system and hollow crystals after removing the disordered core materials and others.

Experimental Section

The synthetic procedure used in this work was adapted by previously reported by Kahr et al.[6] Zinc nitrate hexahydrate (219.5 mg), 2-nitroimidazole (119 mg) and 120.1 mg purine were dissolved upon stirring in DMF (15 mL). Methanol (0.5 mL) was added to the solution, which was then sealed in a Teflon-lined autoclave (40 mL) and incubated at 100 °C for chosen growth times between 1 h and six weeks. The resulting precipitate was collected by centrifugation and washing for several times with methanol. Finally, the powder was left to dry at 60 °C overnight.

Scanning electron microscopy (SEM) was performed on each of the samples by using a JEOL-JSM-6700F field-emission gun microscope, operated between 1 to 5 kV in gentle mode. To avoid damaging the sample, which can occur due to beam charging, each sample was coated with a thin film of gold prior to insertion into the microscope column. For revealing the inner structures of particles, the particles were crushed: the powder sample was deposited in a mortar and suspended in a few drops of acetone before being crushed with a pestle. Transmission electron microscopic (TEM) images of the samples were obtained by a JEOL JEM-2011 electron microscope, operated at an accelerating voltage of 200 kV and fitted with a LaB_6 filament. The images were recorded using a Gatan 794 CCD camera. Powder X-ray diffraction (PXRD) patterns of the different samples were obtained using a PANalytical Empyrean diffractometer, with $Cu_{K\alpha}$ radiation ($\lambda = 1.5418$ Å). A position-sensitive detector with a scan range of 5–40° was used over a period of 1 h to detect the diffracted X-rays. HighScore Plus software was used to analyse the resulting PXRD patterns. For the porosity measurements, the as-prepared samples were heated in vacuum at 120 °C overnight, and then low-pressure gas adsorption (< 0.1 bar) studies were carried out by using a Micromeritics Tristar II instrument for N_2.

Acknowledgements

K.S. and M.T. would like to thank the University of St Andrews for the studentship, Dr. Jürgen Kahr and Professor Paul Wright for their help with this work, Mr. Ross Blackley for his help on

using the SEM and TEM microscopes and Mrs Sylvia Williamson for her assistance with the N_2-adsorption tests. H.F.G. would like to thank EPSRC for the funding (EP/K015540/1). W.Z.Z. thanks EPSRC for the financial support to purchase the FEG SEM (EP/F019580/1).

Keywords: crystal growth · electron microscopy · metal–organic frameworks · zeolitic imidazolate frameworks

[1] a) O. M. Yaghi, M. O'Keeffe, N. W. Ockwig, H. K. Chae, M. Eddaoudi, J. Kim, *Nature* **2003**, *423*, 705; b) S. Kitagawa, R. Kitaura, S. Noro, *Angew. Chem. Int. Ed.* **2004**, *43*, 2334; *Angew. Chem.* **2004**, *116*, 2388; c) G. Férey, *Chem. Soc. Rev.* **2008**, *37*, 191; d) C. B. Aakeröy, N. R. Champness, C. Janiak, *CrystEngComm* **2010**, *12*, 22.

[2] D. Farrusseng, S. Aguado, C. Pinel, *Angew. Chem. Int. Ed.* **2009**, *48*, 7502; *Angew. Chem.* **2009**, *121*, 7638.

[3] Y. Takashima, V. M. Martinez, S. Furukawa, M. Kondo, S. Shimomura, H. Uehara, M. Nakahama, K. Sugimoto, S. Kitagawa, *Nat. Commun.* **2011**, *2*, 1.

[4] P. Horcajada, C. Serre, G. Maurin, N. A. Ramsahye, F. Balas, M. Vallet-Regi, M. Sebban, F. Taulelle, G. Ferey, *J. Am. Chem. Soc.* **2008**, *130*, 6774.

[5] a) X. C. Huang, Y. Y. Lin, J. P. Zhang, X. M. Chen, *Angew. Chem. Int. Ed.* **2006**, *45*, 1557; *Angew. Chem.* **2006**, *118*, 1587; b) K. S. Park, Z. Ni, A. P. Côté, J. Y. Choi, R. Huang, F. J. Uribe-Romo, H. K. Chae, M. O'Keeffe, O. M. Yaghi, *Proc. Natl. Acad. Sci. USA* **2006**, *103*, 10186; c) J. P. Zhang, Y. B. Zhang, J. B. Lin, X. M. Chen, *Chem. Rev.* **2012**, *112*, 1001.

[6] J. Kahr, J. P. S. Mowat, A. M. Z. Slawin, R. E. Morris, D. Fairen-Jimenez, P. A. Wright, *Chem. Commun.* **2012**, *48*, 6690.

[7] B. R. Pimentel, A. Parulkar, E. K. Zhou, N. A. Brunelli, R. P. Lively, *ChemSusChem* **2014**, *7*, 3202.

[8] A. Hayashi, A. P. Côté, H. Furukawa, M. O'Keeffe, O. M. Yaghi, *Nat. Mater.* **2007**, *6*, 501.

[9] V. A. Blatov, G. D. Ilyushin, D. M. Proserpio, *Chem. Mater.* **2013**, *25*, 412.

[10] P. Schierz, S. Fritzsche, W. Janke, S. Hannongbua, O. Saengsawang, C. Chmelik, J. Kärger, *Microporous Mesoporous Mater.* **2015**, *203*, 132.

[11] a) A. Bravais, *Études Crystallographiques*, Gauthier-Villars, Paris, **1866**; b) M. G. Friedel, *Bull. Soc. Fr. Mineral. Cristallogr.* **1907**, *30*, 326; c) J. D. H. Donnay, D. Harker, *Am. Mineral.* **1937**, *22*, 446.

[12] a) W. Ostwald, *Lehrbruck der Allgemeinen Chemie* **1896**, *2*; b) R. Boistelle, J. P. Astier, *J. Cryst. Growth* **1988**, *90*, 14.

[13] P. Hartman, W. G. Perdok, *Acta Crystallogr.* **1955**, *8*, 521.

[14] C. M. Zheng, H. F. Greer, C. Y. Chiang, W. Z. Zhou, *CrystEngComm* **2014**, *16*, 1064.

[15] X. Y. Chen, M. H. Qiao, S. H. Xie, K. N. Fan, W. Z. Zhou, H. Y. He, *J. Am. Chem. Soc.* **2007**, *129*, 13305.

[16] a) H. F. Greer, F. J. Yu, W. Z. Zhou, *Sci. China Chem.* **2011**, *54*, 1867; b) F. J. Yu, W. Z. Zhou, *Prog. Nat. Sci. Mater. Int.* **2013**, *23*, 331; c) K. Self, H. Zhou, H. F. Greer, Z. R. Tian, W. Z. Zhou, *Chem. Commun.* **2013**, *49*, 5411.

[17] a) X. F. Yang, J. X. Fu, C. J. Jin, J. A. Chen, C. L. Liang, M. M. Wu, W. Z. Zhou, *J. Am. Chem. Soc.* **2010**, *132*, 14279; b) H. Q. Zhan, X. F. Yang, C. M. Wang, J. Chen, Y. P. Wen, C. L. Liang, H. F. Greer, M. M. Wu, W. Z. Zhou, *Cryst. Growth Des.* **2012**, *12*, 1247; c) M. L. Moreira, J. Andrés, V. R. Mastelaro, J. A. Varela, E. Longo, *CrystEngComm* **2011**, *13*, 5818.

[18] J. R. G. Sander, D.-K. Bučar, J. Baltrusaitis, L. R. MacGillivray, *J. Am. Chem. Soc.* **2012**, *134*, 6900.

[19] a) W. Z. Zhou, *Adv. Mater.* **2010**, *22*, 3086; b) H. F. Greer, P. S. Wheatley, S. E. Ashbrook, R. E. Morris, W. Z. Zhou, *J. Am. Chem. Soc.* **2009**, *131*, 17986; c) J. F. Yao, D. Li, X. Y. Zhang, C. H. Kong, W. B. Yue, W. Z. Zhou, H. T. Wang, *Angew. Chem. Int. Ed.* **2008**, *47*, 8397; *Angew. Chem.* **2008**, *120*, 8525.

[20] a) S. R. Venna, J. B. Jasinski, M. A. Carreon, *J. Am. Chem. Soc.* **2010**, *132*, 18030; b) J. Cravillon, S. Münzer, S.-J. Lohmeier, A. Feldhoff, K. Huber, M. Wiebcke, *Chem. Mater.* **2009**, *21*, 1410.

[21] P. Scherrer, *Göttinger Nachrichten Gesell.* **1918**, *2*, 98.

[22] J. L. C. Rowsell, O. M. Yaghi, *Angew. Chem. Int. Ed.* **2005**, *44*, 4670; *Angew. Chem.* **2005**, *117*, 4748.

[23] K. M. Choi, H. J. Jeon, J. K. Kang, O. M. Yaghi, *J. Am. Chem. Soc.* **2011**, *133*, 11920.

[24] L. J. Murray, M. Dincă, J. R. Long, *Chem. Soc. Rev.* **2009**, *38*, 1294.

[25] a) P. Curie, *Bull. Soc. Fr. Mineral. Cristallogr.* **1885**, *8*, 145; b) G. Z. Wulff, *Kristallografiya* **1901**, *54*, 449.

Received: August 28, 2015
Published online on November 18, 2015

